Korean J. Chem. Eng., 32(8), 1498-1514 (2015)
DOI: 10.1007/s11814-014-0361-3

pISSN: 0256-1115
eISSN: 1975-7220

Lattice Boltzmann analysis of effect of heating location and Rayleigh number on natural convection in partially heated open ended cavity

Krunal Madhukar Gangawane, Ram Prakash Bharti†, and Surendra Kumar

Department of Chemical Engineering, Indian Institute of Technology Roorkee, Roorkee -247 667, Uttarakhand, India
(*Received 20 March 2014 • accepted 5 December 2014*)

Abstract–Natural convection characteristics of a partially heated open ended square cavity have been investigated numerically by using an in-house computational flow solver based on the passive scalar thermal lattice Boltzmann method (PS-TLBM) with *D*2*Q*9 (two-dimensional and nine-velocity link) lattice model. The partial part of left wall of the cavity is heated isothermally at either of the three different (bottom, middle and top) locations for the fixed heating length as half of characteristic length (*H*/2) while the right wall is open to the ambient conditions. The other parts of the cavity are thermally isolated. In particular, the influences of partial heating locations and Rayleigh number ($10^3 \leq Ra \leq 10^6$) in the laminar zone on the local and global natural convection characteristics (such as streamline, vorticity and isotherm contours; centerline variations of velocity and temperature; and local and average Nusselt numbers) have been presented and discussed for the fixed value of the Prandtl number (Pr=0.71). The streamline patterns show qualitatively similar nature for all the three heating cases and Rayleigh numbers, except the change in the recirculation zone which is found to be largest for middle heating case. Isotherm patterns are shifted towards a partially heated wall on increasing Rayleigh number and/or shifting of heating location from bottom to top. Both the local and average Nusselt numbers, as anticipated, shown proportional increase with Rayleigh number. The cavity with middle heating location shown higher heat transfer rate than that for the top and bottom heating cases. Finally, the functional dependence of the average Nusselt number on flow governing parameters is also presented as a closure relationship for the best possible utilization in engineering practices and design.

Keywords: Natural Convection, Passive Scalar Thermal Lattice Boltzmann Method (PS-TLBM), Partially Heated Open Ended Cavity, Nusselt Number, Rayleigh Number

INTRODUCTION

The study of heat transfer enhancement is considered as an important and essential phenomenon [1] from the fundamental and pragmatic point of view. An investigation of the natural convection heat transfer in closed as well as open ended cavity encompasses great scientific interest due to its wide ranging applications in domestic as well as industrial fields [2-5], in scientific/engineering practices, viz., chemical vapor deposition [6], cooling devices in electronic equipment [7-9], polymer processing [10], material processing [11], solar collectors [12], etc.

The thermal control of electronic devices represents novel topic in convective heat transfer phenomenon. In wide range of industrial applications, electronic devices play vital role. The cooling of these devices can be achieved by natural and mixed convection. In such cases, one of the important aspects of thermal control is optimum placement of the discrete heaters at appropriate positions (i.e., optimum heating position) such that the circulating air through ventilation ports provides the most efficacious cooling in these devices [7]. Further, application of natural convection in cooling of electronic equipments (mostly low power systems, such as TV and DVD players) is achieved by providing number of vents on the cover cases of these systems. These vents are provided for ambient air to enter and hot air to leave the case. The location and size of these vents should be optimum for efficient heat transfer [13]. In addition, the departure from the basic condition (i.e., cavity walls maintained isothermally) is quite often encountered in practical situations [14]. Study of heat transfer characteristics in such devices subjected to partial heating is must. The present work, thus, aims to numerically elucidate the influence of heating locations (top, middle and bottom) of a partially heated (constant heater size) wall on the heat and fluid flow characteristics of open ended square cavity using the lattice Boltzmann method (LBM).

Over the years, the mesoscopic numerical approach, namely, lattice Boltzmann method (LBM), has proven to be one of the potential and prominent computational tool for the efficient solution of the wide ranges of complex physical phenomenon involving the interfacial dynamics and complex boundaries [15-17]. The fundamental idea of LBM is to solve simplified kinetic models, which include the essential physics of microscopic (or mesoscopic) processes in such a way that the microscopic averaged properties are suitable representation of the desired macroscopic equations. These models in an unambiguous way are the discrete distribution functions or population f (**x**, t)=f (**x**, **e**, t) which represents the probability of finding a particle movement with lattice speed 'e' at position 'x' and at time 't'. For the solution of the thermal energy equation by using LBM, three approaches, namely, multispeed [18], double distribution function (DDF) [19] and passive scalar (PS) [20], are

†To whom correspondence should be addressed.
E-mail: rpbharti@iitr.ac.in
Copyright by The Korean Institute of Chemical Engineers.

efficiently utilized in the available literature. In the multispeed approach [18], temperature can be obtained by expanding equilibrium distribution function to the third order of velocity. It is, however, least popular approach due to disadvantages such as Galilean invariance, constant Prandtl number (≈0.5) and severe numerical instability (as higher order velocity terms are involved) [21]. Subsequently, He et al. [19] proposed double distribution function (DDF) or internal energy distribution function approach. It utilizes the two different distribution functions, one each, for the estimation of flow and thermal fields. It is proven to be much better in terms of numerical stability and efficiency for the wider range of temperature and Prandtl numbers [21-23]. It is, however, unfavorable as the simplicity of LBM is lost due to the involvement of compression work done by pressure and viscous heat dissipation [21].

Further, Peng et al. [20] presented a passive scalar (PS) approach which is simplified version of DDF approach [19]. In this approach, temperature is assumed to be passive scalar and is advected by the flow field. The macroscopic temperature equation is similar to a passive scalar evolution equation, if the viscous heat dissipation and compression work done by pressure are negligible. This approach possesses better numerical stability, over other two approaches, in yielding the efficient solution over the broad range of Prandtl number and the simplicity of LBM is also retained [21-23]. The passive scalar thermal lattice Boltzmann method (PS-TLBM) is, therefore, used herein for the estimation of natural convection flow and heat transfer characteristics of a partially heated open ended square cavity. Before presenting the new results obtained in this work, it is utile to recollect the limited available results on the natural convection in open ended cavity.

The natural convection in the cavities of varying configurations (viz., differentially heated, open ended, inclined and lid driven, etc.) has been extensively explored well over the last few decades. Extensive literature is now available for the convective heat transfer mechanism in an open ended heated cavity, however, very limited results of the convection in an open ended cavity with partial and/or non-uniform heating wall/walls are available. For instance, Shin and Economou [24] have studied the mass transfer by both natural and forced convection in an open rectangular cavity ($0.5 \le AR \le 4.0$) for lower ranges of Schmidt ($Sh \le 10^3$) and Rayleigh ($Ra \le 10^3$) numbers. The symmetric flow and concentration fields were observed [24] at the initial time followed by the symmetry breaking and oscillatory flows. Subsequently, Vafai and Ettefagh [25] have investigated the heat and fluid flow instabilities in buoyancy driven open-ended cavity for the broad range of Rayleigh number ($10^3 \le Ra \le 9\times10^5$). They observed asymmetric sinusoidal and distorted W-shaped oscillations in the range of Rayleigh number as ($3.5\times10^5 \le Ra \le 5.5\times10^5$) and ($6\times10^5 \le Ra \le 9\times10^5$), respectively. Later, substantial effects of surface radiation on the flow and thermal behaviors were observed [26] in the numerically investigation of natural convection in an open ended cavity in the range of Rayleigh number as ($10^4 \le Ra \le 10^8$). Mohamad [27] has studied the natural convection in an open ended rectangular cavity for various physical flow governing parameters such as inclination angle ($10^o \le \phi \le 90^o$), Rayleigh number ($10^3 \le Ra \le 10^7$), aspect ratio ($0.5 \le AR \le 2.0$) and Prandtl number (Pr=0.71) by using the control volume, finite difference method based on SIMPLER algorithm. They observed slight change in heat transfer rate with the change in inclination angle, however, flow instability was observed at high Rayleigh number and low inclination angle. Subsequently, Angirasa et al. [28] used stream function-vorticity formulation to analyze the natural convection in an isothermal open ended cavity for the wide range of Grashof number ($10^4 \le Gr \le 10^7$) at constant Prandtl number (Pr=0.71). The unsteadiness in the convective flow was reported at moderate to high Grashof numbers. Khanafer and Vafai [29,30] have investigated the heat and fluid flow characteristics of open ended cavity. Their main thrust was the accurate representation of the open ended boundary conditions for two-and three-dimensional enclosures. The numerical investigation of laminar natural convection ($10^3 \le Ra \le 10^6$) in shallow rectangular cavity ($1 \le AR \le 0.125$) has also been carried out by Polat and Bilgen [31]. Similarly, Hinojosa et al. [32] have numerically elucidated the effect of Rayleigh number ($10^4 \le Ra \le 10^7$) on the natural convective heat transfer and surface thermal radiation in a tilted ($0^o \le \phi \le 180^o$) open ended square cavity. They reported substantial change in the convective Nusselt number with the inclination angle, however, radiative Nusselt number shown negligible dependence on the inclination angle.

Further, Bilgen and Oztop [33] have investigated the thermal and hydrodynamic nature of a partially open inclined ($0^o \le \phi \le 120^o$) square cavity (adiabatic walls and a partial opening of aperture opening in the range as 0.25-0.75) for the broad range of the Rayleigh number ($10^3 \le Ra \le 10^6$). The volumetric flow rate and Nusselt number was reported to be directly proportional with Rayleigh number, inclination angle and aperture size. The numerical investigation of natural convection ($10^4 \le Ra \le 10^6$) in an open ended rectangular cavity ($0.5 \le AR \le 10$) has been carried out by using thermal lattice Boltzmann method (TLBM) [34]. They reported inverse dependence of the rate of heat transfer on the aspect ratio based on the use of *D*2*Q*9 and *D*2*Q*4 lattice models for the flow and thermal fields, respectively. Similarly, Sajjadi et al. [35] investigated the effects of inclination angle ($-45^o \le \phi \le 45^o$) and Rayleigh number ($10^3 \le Ra \le 10^6$) on natural convection in the cavity by using LBM. They observed increase in rate of heat transfer for the lower inclination angle ($-45^o \le \phi \le 0^o$), whereas reverse trend is observed for higher inclination angle ($0^o \le \phi \le 45^o$).

In addition, natural convection losses from the three dimensional open ended inclined ($0^o \le \phi \le 90^o$) cavity of various shapes (viz., spherical, cubical and hemispherical) have been done by Prakash et al. [36]. For the opening ratio (1, 0.5, 0.25) and Rayleigh number ($4\times10^4 \le Ra \le 2.5\times10^9$), the hemispherical open cavity shown highest natural convection loss than other two shapes. The dependence of mixed convection phenomenon induced by vibrations (in vertical direction) in an open ended cavity filled with porous medium on the flow governing parameters (vibrational Reynolds number, modified Rayleigh number and Darcy number) has been elucidated by Chung and Vafai [37]. At higher Reynolds and Darcy numbers, vibrational effects on thermal and hydrodynamic behaviors in cavity are found to be more significant. They further emphasized the use of generalized model at higher values of vibrational Reynolds number and modified Rayleigh number. Subsequently, Haghshenas et al. [38] have used least square based Lattice Boltzmann method (LBM) to investigate the natural convection ($10^3 \le Ra \le 10^6$, Pr=1) heat transfer in an open ended cavity filled with porous material

(Darcy number Da=0.01, and porosity of medium as $0.4 \leq \varepsilon \leq 0.9$). The rate of heat transfer has shown proportional increase with Rayleigh number and porosity of medium. Recently, Kefayati [39] studied the influence of magnetic field (Hartmann number as $0 \leq Ha \leq 90$) on natural convection ($10^4 \leq Ra \leq 10^6$) in an open ended cavity filled with nanofluid (volume fraction of nanoparticles as 0-0.06) by using LBM. They have reported a decrease in the rate of heat transfer with increase in Hartmann number.

Based on foregoing elucidation of available literature, it is, thus, safe to conclude that the conventional computational fluid dynamic (CFD) tools as well as lattice Boltzmann method (LBM) have been successfully utilized, over the decades, to investigate the convective flow characteristics of an open ended cavity. However, most of studies have considered completely heated wall of open ended cavity. To the best of our knowledge, none of the study have considered partially heated wall of cavity whose opposite end is open to the ambient.

In several industrial applications (e.g., cooling of electronic components and solar heat collectors), however, the active walls may be subject to abrupt temperature variations due to shading effects, etc. The relative position of the partial heater on the system wall has significant influence on the flow and heat transfer characteristics [40]. Also the partial heaters are basically used for cooling of electronic equipment by means of natural convection phenomenon [41]. Additionally, the temperature difference and characteristic length should be $\Delta T \leq 100\ ^{\circ}C$ and $H \leq 0.5$ m, respectively, for natural convective heat transfer in cooling of the electronic devices to be in laminar regime [13]. Thus, study of optimum location of partial heaters in cavities (closed as well as open) is important owing to its industrial as well as pragmatic significance. This constitutes the main aim of the present study to investigate the influence of partial heater on laminar natural convective heat transfer characteristics. In particular, the influences of location of partially heating (middle, top and bottom) of left wall of open ended cavity on thermal and fluid flow characteristics have been examined for the wide range of Rayleigh number ($10^3 \leq Ra \leq 10^6$) at constant Prandtl number (Pr=0.71) by using the passive scalar thermal lattice Boltzmann method (PS-TLBM).

PROBLEM STATEMENT AND MATHEMATICAL MODELING

Consider a steady, laminar, natural convection in an incompressible fluid from an open ended square cavity (aspect ratio, AR=L/H=1 where L and H are cross-sectional length and height, respectively), as shown in Fig. 1. The partial part of left wall (x=0) of cavity is heated isothermally (with heating length of l_h<H at temperature T_H) at either of the three, viz., (i) top (ii) middle and (iii) bottom heating locations. The length of heated part of left wall (x=0) is kept constant (l_h=H/2) in this study. The right wall (x=L) of cavity is, however, open to the ambient conditions (temperature T_C<T_H). The remaining part of left wall, bottom (y=0) and top (y=H) walls of cavity are maintained adiabatically, i.e., thermally insulated. The thermo-physical properties (namely, viscosity μ, thermal conduc-

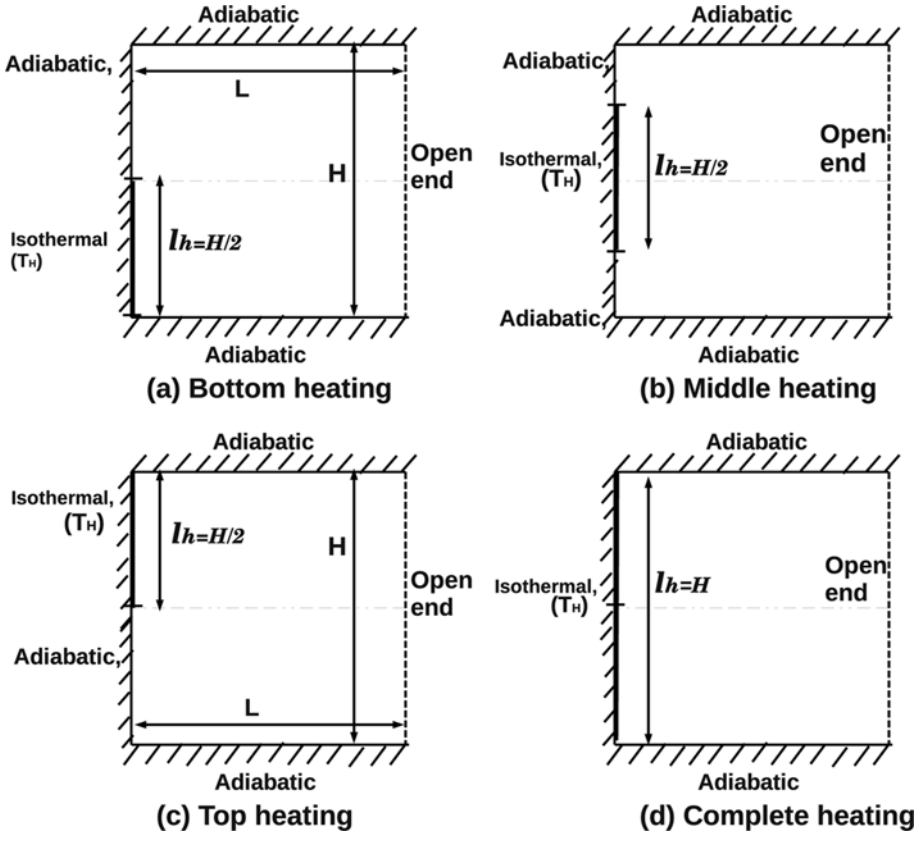

Fig. 1. Schematic representation of the computational domain (i.e., open ended cavity) with boundary conditions.

tivity κ, heat capacity c_p, etc.) of the working Newtonian fluid (air, Pr=0.71) are considered to be independent of the temperature (T), except that of fluid density (ρ) appearing in the body force term in the Navier-Stokes equation. Evidently, each fluid shows varying extent of the dependence of density on temperature [42-44]. The well-known Boussinesq approximation is commonly used [45] to account for the small to moderate variations in the density. It is expressed as $\rho=\overline{\rho}\,[1-\beta(T-\overline{T})]$, where β is coefficient of volumetric expansion at constant pressure and $\overline{\rho}$ is fluid density at a reference temperature ($\overline{T}$, i.e., average fluid temperature) [20,45,46]. While this approximation is customarily arouse to maintain the level of complexity at a traceable level in the convective flow studies [20,45], it evidently couples the flow and thermal fields which requires simultaneous solution of the governing equations. Furthermore, the viscous heat dissipation, radiation heat transfer and compression work done by pressure are assumed to be negligible. The assumptions of constant thermo-physical properties and negligible viscous heat dissipation lead to decouple the momentum and energy equations. These approximations, however, restrict [20] the applicability of numerical results to the situations where the temperature difference ($\Delta T=T_H-T_C$) is not too large and/or for moderate viscosity and/or shearing levels so that the viscous dissipation effects are negligible. The literature [13,46] suggests that the thermophysical properties (heat capacity, thermal conductivity, viscosity, etc) of air are independent of tempterature for the maximum temperature difference of $\Delta T\leq 60\ ^{\circ}C$. The temperature difference (ΔT) herein is maintained sufficiently small to justify the accountability of the variation of the fluid viscosity with temperature.

Under the above-noted assumptions/approximations, a simplified form of the natural convection flow governing equations in conjunction with Boussinesq approximation, namely, continuity, Navier-Stokes and thermal energy equations are given as follow:

$$\frac{\partial u_x}{\partial x}+\frac{\partial u_y}{\partial y}=0 \quad \text{(continuity)} \tag{1}$$

$$\rho\left(u_x\frac{\partial u_x}{\partial x}+u_y\frac{\partial u_x}{\partial y}\right)=-\frac{\partial p}{\partial x}+\mu\left(\frac{\partial^2 u_x}{\partial x^2}+\frac{\partial^2 u_x}{\partial y^2}\right) \quad \text{(x-momentum)} \tag{2}$$

$$\rho\left(u_x\frac{\partial u_y}{\partial x}+u_y\frac{\partial u_y}{\partial y}\right)=-\frac{\partial p}{\partial y}+\mu\left(\frac{\partial^2 u_y}{\partial x^2}+\frac{\partial^2 u_y}{\partial y^2}\right)+\rho g_y\beta(T-\overline{T}) \quad \text{(y-momentum)} \tag{3}$$

$$\rho c_p\left(u_x\frac{\partial T}{\partial x}+u_y\frac{\partial T}{\partial y}\right)=\kappa\left(\frac{\partial^2 T}{\partial x^2}+\frac{\partial^2 T}{\partial y^2}\right) \quad \text{(thermal energy)} \tag{4}$$

The physically consistent boundary conditions for the present problem (Fig. 1) are written as

- The left wall (x=0) is considered as no-slip stationary wall. It is, however, partially heated isothermally (temperature T_H) for the fixed length of heating (l_h=H/2) at either of the three (top, middle and bottom) locations, i.e.,

$$u_x=0,\ u_y=0 \text{ and } \begin{cases} \dfrac{\partial T}{\partial x}=0 & \text{for } h_1(\neq 0)\geq y\geq 0 \\ T=T_H & \text{for } h_1\leq y\leq h_2 \\ \dfrac{\partial T}{\partial x}=0 & \text{for } h_2(\neq H)\leq y\leq H \end{cases} \tag{5}$$

where, the lengths h_1 and $h_2=(h_1+l_h)$ are defined for the different cases (Fig. 1) as follow:

(a) In the case of bottom heating, the heater of length (l_h) is placed in the bottom portion of the wall whereas the upper portion is maintained adiabatically. Therefore,

$h_1=0$ and $h_2=H/2$

(b) In case of middle heating, the heater of length (l_h) is placed in the middle section of the wall whereas the lower and upper portions are maintained adiabatically. Therefore,

$h_1=H/4$ and $h_2=3H/4$

(c) In the case of top heating, the heater of length (l_h) is placed in the upper portion of the wall whereas the lower portion is maintained adiabatically. Therefore,

$h_1=H/2$ and $h_2=H$

- Right wall (x=L) is open to the ambient conditions, i.e.,

$$\frac{\partial u_x}{\partial x}=0,\ \frac{\partial u_y}{\partial x}=0 \text{ and } \begin{cases} T=T_C & \text{if } u_x<0 \\ \dfrac{\partial T}{\partial x}=0 & \text{if } u_x>0 \end{cases} \tag{6}$$

- Bottom (y=0) and top (y=H) walls are no-slip stationary walls maintained adiabatically, i.e.,

$$u_x=0,\ u_y=0,\ \text{and } \frac{\partial T}{\partial y}=0 \tag{7}$$

where, (x, y), (u_x, u_y), p, ρ, κ, c_p, μ and T are Cartesian directions, velocity components, pressure, density of fluid, thermal conductivity, specific heat capacity, dynamic viscosity and temperature, respectively.

The above noted governing differential equations (Eqs. (1)-(4)) and boundary conditions (Eqs. (5)-(7)) are made dimensionless by using the reference length (H), reference velocity (U), reference pressure (ρU^2) and reference temperature $(T-T_C)/(T_H-T_C)$ to scale the lengths, velocities, pressure and temperature, respectively. The dimensionless (variables with * superscript) form of governing equations (Eqs. (1)-(4)) can, then, be written as follow.

$$\frac{\partial u_x^*}{\partial x^*}+\frac{\partial u_y^*}{\partial y^*}=0 \tag{8}$$

$$u_x^*\frac{\partial u_x^*}{\partial x^*}+u_y^*\frac{\partial u_x^*}{\partial y^*}=-\frac{\partial P^*}{\partial x^*}+\frac{1}{\Gamma_m}\left(\frac{\partial^2 u_x^*}{\partial x^{*2}}+\frac{\partial^2 u_x^*}{\partial y^{*2}}\right)$$

$$\text{where } \Gamma_m=\sqrt{Gr}=\sqrt{\frac{Ra}{Pr}} \tag{9}$$

$$u_x^*\frac{\partial u_y^*}{\partial x^*}+u_y^*\frac{\partial u_y^*}{\partial y^*}=-\frac{\partial P^*}{\partial y^*}+\frac{1}{\Gamma_m}\left(\frac{\partial^2 u_y^*}{\partial x^{*2}}+\frac{\partial^2 u_y^*}{\partial y^{*2}}\right)+T^* \tag{10}$$

$$u_x^*\frac{\partial T^*}{\partial x^*}+u_y^*\frac{\partial T^*}{\partial y^*}=\frac{1}{\Gamma_e}\left(\frac{\partial^2 T^*}{\partial x^{*2}}+\frac{\partial^2 T^*}{\partial y^{*2}}\right) \quad \text{where } \Gamma_e=\Gamma_m\times Pr \tag{11}$$

Similarly, the boundary conditions (Eqs. (5)-(7)) in the dimensionless form can be expressed as follow.

• At the left ($x^*=0$) wall,

$$u_x^*=0,\ u_y^*=0 \text{ and } \begin{cases} \dfrac{\partial T^*}{\partial x^*}=0 & \text{for } h_1^*(\neq 0)\geq y^*\geq 0 \\ T^*=1 & \text{for } h_1^*\leq y\leq h_2^* \\ \dfrac{\partial T^*}{\partial x^*}=0 & \text{for } h_2^*(\neq 1)\leq y^*\leq 1 \end{cases} \tag{12}$$

where, h_1^* and $h_2^*=(h_1^*+L_h)$ are dimensionless lengths given as follow for the different cases of heating arrangements. The L_h ($=l_h/H=1/2$) being the dimensionless length of the heating section. The lengths (h_1^*, h_2^*) equal to (0, 1/2), (1/4, 3/4) and (1/2, 1) for the bottom, middle and top heating locations, respectively.

• At the right ($x^*=1$) wall,

$$\frac{\partial u_x^*}{\partial x^*}=0,\ \frac{\partial u_y^*}{\partial x^*}=0 \text{ and } \begin{cases} T^*=0 & \text{if } u_x^*<0 \\ \dfrac{\partial T^*}{\partial x^*}=0 & \text{if } u_x^*>0 \end{cases} \tag{13}$$

• At the bottom ($y^*=0$) and top ($y^*=1$) walls,

$$u_x^*=0,\ u_y^*=0,\ \text{and } \frac{\partial T^*}{\partial y^*}=0 \tag{14}$$

The dimensionless groups, namely, Prandtl number (Pr), Grashof number (Gr) and Rayleigh number (Ra) appearing in the dimensionless equations (Eqs. (9)-(11)) are defined as

$$\mathrm{Pr}=\frac{c_p\mu}{\kappa}=\frac{\nu}{\alpha};\ \mathrm{Gr}=\frac{g\beta\Delta T H^3}{\nu^2} \text{ and } \mathrm{Ra}=\mathrm{Gr}\times\mathrm{Pr}=\frac{g\beta\Delta T H^3}{\alpha\nu} \tag{15}$$

where ν and α being the kinematic viscosity and thermal diffusivity of the fluid, respectively. Since the characteristic velocity (U) used in the above non-dimensionalization is not known, the determination of characteristic velocity is an important step in natural convection problem [46]. In case of natural convection, the reference velocity (U) is approximated [21,34,46-48] as

$$U=\sqrt{g\beta\Delta T H} \text{ or } U=\frac{\nu}{H}\sqrt{\frac{Ra}{Pr}} \tag{16}$$

The numerical solution of the flow governing equations (Eqs. (1)-(4) or Eqs. (8)-(11)) in conjunction with the physically consistent boundary conditions (Eqs. (5)-(7) or Eqs. (12)-(14)) produces the pressure, velocity and thermal fields. These fully converged flow and thermal fields are further used to obtain the local and global flow characteristics (such as streamlines, vorticity, pressure and drag coefficients, local and average Nusselt numbers, etc.). In the present study, the derived flow and thermal variables (namely, streamlines, vorticity, local and average Nusselt numbers) used are defined as follow:

• Stream function (ψ) and vorticity (ζ) field are evaluated by using

$$\psi=\int u_x dy \tag{17}$$

$$\zeta=\frac{\partial u_y}{\partial x}-\frac{\partial u_x}{\partial y} \tag{18}$$

• The dimensionless rate of heat transfer, i.e., Nusselt number (Nu), is generally considered as one of the important parameter in the quantification and analysis of the heat transfer enhancement and characteristics. The local Nusselt number (Nu) can be defined [23,49-53] as,

$$\mathrm{Nu}=-\frac{H}{\Delta T}\frac{\partial T}{\partial n}\bigg|_{x=0} \text{ or } \mathrm{Nu}=-\frac{1}{\Delta T^*}\frac{\partial T^*}{\partial n^*}\bigg|_{x'=0} \tag{19}$$

where n is inward direction normal to wall. The local values of the Nusselt number can then be averaged over the surface to determine the overall heat transfer, i.e., average Nusselt number ($\overline{\mathrm{Nu}}$), as

$$\overline{\mathrm{Nu}}=\frac{1}{H}\int_0^H \mathrm{Nu}\ dS \text{ or } \overline{\mathrm{Nu}}=\int_0^1 \mathrm{Nu}\ dS^* \tag{20}$$

Henceforth, the dimensionless variables (u_x^*, u_y^*, T^*, P^*, x^*, y^*, etc.) have been used to present the new results. The subsequent section details the numerical methodology and computational algorithm adopted herein.

NUMERICAL SOLUTION METHODOLOGY

In this work, the numerical solution of the governing equations in conjunction with the physically realistic boundary conditions has been obtained by using a passive scalar thermal lattice Boltzmann method (PS-TLBM) based computational flow solver. The solver is developed in-house by the present authors in C++ programming language. The PS-TLBM is detailed herein the ensuing section.

1. Passive Scalar Thermal Lattice Boltzmann Method (PS-TLBM)

LBM originates from the kinetic Boltzmann equation, which can be obtained by expanding the basic formulation of lattice gas automata to real particle distribution functions. The classical approaches of solving the fluid flow problems involve the second (or higher) order partial differential equations (PDEs). In contrast to classical approaches, LBM utilizes only first order PDE, i.e., Boltzmann equation, which is expressed as [54],

$$\frac{\partial f}{\partial t}+e\cdot\nabla f=-\frac{1}{\tau}(f-f^{eq}) \quad \text{(Boltzmann equation)} \tag{21}$$

The distribution functions (DFs) in LBM, used to represent the particles, are obtained by the solution of lattice Boltzmann equation (LBE), i.e., spatial discretized form of kinetic Boltzmann equation [16,20,54,55]. In the passive scalar approach, two different distribution functions, f_k and g_k, are used to estimate the flow and thermal fields, respectively, in the lattice link direction 'k'. A time integration of the Boltzmann equation (Eq. (21)) in any direction 'k' results in the basic LBE. The basic form of LBE for the flow and thermal fields is presented below.

1-1. Basic Form of LBE for Flow and Thermal Energy Fields

The passive scalar approach [20,55] segregates the flow and thermal energy fields with the approximation of negligible viscous heat dissipation and pressure compression work. It utilizes two separate distribution functions, f_k and g_k, to obtain the flow and thermal fields, respectively. The lattice Boltzmann equations (LBE) for the flow and thermal energy transports are written as follow:

$$f_k(\mathbf{x}+\Delta\mathbf{x}, t+\Delta t)-f_k(\mathbf{x}, t)=-\frac{1}{\tau_\nu}[f_k(\mathbf{x}, t)-f_k^{eq}(\mathbf{x}, t)]+\Delta t F_k \quad (22)$$

$$g_k(\mathbf{x}+\Delta\mathbf{x}, t+\Delta t)-g_k(\mathbf{x}, t)=-\frac{1}{\tau_g}[g_k(\mathbf{x}, t)-g_k^{eq}(\mathbf{x}, t)] \quad (23)$$

where, the equilibrium distribution functions (f_k^{eq} and g_k^{eq} for the flow and thermal fields, respectively) are given as

$$f_k^{eq}(\mathbf{x}, t)=\rho w_k\left[1+\frac{3(\mathbf{u}\cdot\mathbf{e}_k)}{c^2}+\frac{9(\mathbf{u}\cdot\mathbf{e}_k)^2}{2c^4}+\frac{3(\mathbf{u}\cdot\mathbf{u})}{2c^2}\right] \quad (24)$$

$$g_k^{eq}(\mathbf{x}, t)=T w_k\left[1+\frac{3(\mathbf{u}\cdot\mathbf{e}_k)}{c^2}\right] \quad (25)$$

Here, Δt, Δx ($=\mathbf{e}_k\Delta t$), c ($=\Delta x/\Delta t=1.0$), $\mathbf{u}$, T, $\mathbf{e}_k$ and w_k are lattice time step, lattice space step, lattice streaming speed, velocity vector, temperature, discrete velocity vector and equilibrium distribution of weight for direction k, respectively. The relaxation parameters (τ_ν and τ_g for the momentum and thermal energy transport fields, respectively) are defined as

$$\tau_\nu=3\nu+\frac{1}{2} \quad (26)$$

$$\tau_g=3\alpha+\frac{1}{2} \quad (27)$$

Under the assumptions that the buoyancy force is directly proportional to the temperature gradient and negligible radiative heat transfer, the Boussinesq approximation is accounted [5,34,47,48] by calculating the buoyancy force in the vertical direction as follow.

$$F_k=3w_k g_y \beta\Delta T \quad (28)$$

For *D2Q9* lattice model (two-dimensional, nine velocity link model), w_k and $\mathbf{e}_k$ are represented as,

$$w_k=\begin{cases}4/9 & \text{for } k=0\\ 1/9 & \text{for } k=1, 2, 3, 4\\ 1/36 & \text{for } k=5, 6, 7, 8\end{cases} \quad (29)$$

$$\left.\begin{array}{lll}\mathbf{e_6}=(-1, 1), & \mathbf{e_2}=(0, 1), & \mathbf{e_5}=(1, 1)\\ \mathbf{e_3}=(-1, 0), & \mathbf{e_0}=(0, 0), & \mathbf{e_1}=(1, 0)\\ \mathbf{e_7}=(-1, -1), & \mathbf{e_4}=(0, -1), & \mathbf{e_8}=(1, -1)\end{array}\right\} \quad (30)$$

The macroscopic quantities such as density (ρ), velocity ($\mathbf{u}$) and temperature (T) fields are, then, calculated by using the following relations.

$$\rho=\sum_k f_k;\ \ \rho\mathbf{u}=\sum_k f_k e_k \ \text{ and } \ T=\sum_k g_k \quad (31)$$

The use of Champman-Enskog analysis has proved [19,20,54,55] that the mass, momentum and energy conservation equations can be recovered up to second order from the LBE of momentum and thermal transport (Eqs. (22) and (23)), respectively.

The evolution of LBE takes place in the two successive steps, viz., collision and streaming, as detailed below.

- In *collision step*, the distribution functions are relaxed towards equilibrium state [16,54], as

$$\bar{f}_k(\mathbf{x}, t+\Delta t)=f_k(\mathbf{x}, t)-\frac{1}{\tau_\nu}[f_k(\mathbf{x}, t)-f_k^{eq}(\mathbf{x}, t)] \quad (32)$$

$$\bar{g}_k(\mathbf{x}, t+\Delta t)=g_k(\mathbf{x}, t)-\frac{1}{\tau_g}[g_k(\mathbf{x}, t)-g_k^{eq}(\mathbf{x}, t)] \quad (33)$$

- In *streaming step*, the fluid particles are streamed from one cell to a neighboring cell according to the lattice velocity of the fluid particles in this cell [16,54], as

$$f_k(\mathbf{x}+\Delta\mathbf{x}, t+\Delta t)=\bar{f}_k(\mathbf{x}, t+\Delta t) \quad (34)$$

$$g_k(\mathbf{x}+\Delta\mathbf{x}, t+\Delta t)=\bar{g}_k(\mathbf{x}, t+\Delta t) \quad (35)$$

2. Implementation of Boundary Conditions

An accurate representation and suitable implementation of boundary conditions is one of crucial, as well as important, step in the development of the numerical solvers. The conventional CFD tools use macroscopic variables on boundaries. In LBM, however, boundary conditions are specified by unknown distribution functions directing towards the flow field. For the representation of boundary conditions of the flow field, the estimation of unknown distribution functions on the boundary is accomplished by known wall velocity. The estimation of distribution function for the thermal field is carried out in similar way as that of flow field, and the wall temperature is used for the calculation of unknown distribution functions [21]. For no-slip boundaries, bounce back method of non-equilibrium distribution function [56] is widely used. In the bounce back condition, particle distribution functions moving towards solid boundary bounces back to their original positions.

The unknown distribution function at the no-slip (i.e., left, south and north walls in the present study) boundary of the computational domain is estimated by using the bounce back method as follow.

$$f_k-f_k^{eq}=f_{\hat{k}}-f_{\hat{k}}^{eq} \ \text{ and } \ g_k-g_k^{eq}=g_{\hat{k}}-g_{\hat{k}}^{eq} \quad (36)$$

The flow field boundary condition at the open end (i.e., right wall) of cavity [34] is implemented as below.

$$f_{3, n_x}=f_{3, n_x-1},\ \ f_{6, n_x}=f_{6, n_x-1} \ \text{ and } \ f_{7, n_x}=f_{7, n_x-1} \quad (37)$$

where, n_x is boundary node on the open end (x=L) side. For the implementation of thermal boundary condition at the open end (i.e., right wall) of the cavity, special treatment is required due to the unknown direction of advected velocity. Therefore, depending on the direction of advected velocity, there are two possible ways of treatment of the thermal boundary condition implementation at the open end. If the flow penetration in cavity is taking place then the temperature at the open end is assumed to be ambient. Otherwise, negligible diffusion (i.e., negligible temperature gradient) is another way to implement the thermal boundary condition at the open end [34,38]. For the open end, thus, the unknown distribution functions for the thermal field are evaluated as,

$$\begin{array}{l}g_{3, n_x}=-g_{1, n_x};\ \ g_{6, n_x}=-g_{8, n_x};\ \ g_{7, n_x}=-g_{5, n_x} \ \text{ for } \ u_x<0\\ g_{3, n_x}=g_{3, n_x-1};\ \ g_{6, n_x}=g_{6, n_x-1};\ \ g_{7, n_x}=g_{7, n_x-1} \ \text{ for } \ u_x>0\end{array} \quad (38)$$

3. Numerical Algorithm

The computational algorithm of passive scalar thermal lattice Boltzmann method (PS-TLBM), implemented and developed in C++ programming language, is given as follow:

1. Initialization of the density (ρ>0), velocity (u_x=0, u_y=0), and temperature (T=T_c).

2. Determination of equilibrium distribution functions (f_k^{eq} and g_k^{eq}) by using the values initialized in step (1).

3. To start with, distribution functions and equilibrium distribution functions are set equal to their part, i.e., f_k=f_r^{eq} and g_k=g_k^{eq}.

4. Sequential determination of flow field followed by the thermal field

(a) Collision step (Eqs. (32) and (33)).

(b) Streaming step (Eqs. (34) and (35)).

(c) Updating of boundary conditions (Eqs. (37) and (38)).

(d) Estimation of macroscopic quantities (Eq. (31))

5. Check for the convergence criterion (Eq. (39))

(a) If satisfied, go to step (6).

(b) Else, repeat steps (4) to (5).

6. Process the flow and thermal fields to estimate the local and global characteristic.

The absolute error (ε; Eq. (39)) criterion has been used to check the convergence of numerical solution.

$$\varepsilon_{max} = \max\left|\phi_i^{new} - \phi_i^{old}\right|_{i=1}^{N} \le 10^{-9} \tag{39}$$

where, ϕ represents physical flow variables (i.e., velocity components u_x, u_y, and temperature T) checked for convergence and N is the number of lattice nodes in the computational domain. The superscripts 'new' and 'old' represent for the flow variables calculated at the present and previous time/iterative calculation steps.

RESULTS AND DISCUSSIONS

In this work, the natural convection flow and heat transfer characteristics of a partially heated open ended square cavity are investigated by using the PS-TLBM (with *D2Q9* lattice link model) based in-house computational flow solver. The numerical computations are carried out for the fixed length of isothermal heating (L_h=1/2) at any of the heating location (top, middle and bottom) on the partially heated wall and for the laminar range of the Rayleigh number ($10^3 \le Ra \le 10^6$) varied in logarithmic manner at a fixed value of the Prandtl number (Pr=0.71). The simulations are also performed for the completely isothermally heated (L_h=1) left wall for the comparison purpose. Extensive results encompassing the influences of the heating location and Rayleigh number (Ra) on the local and global flow and heat transfer characteristics (such as streamline, vorticity and isotherm contours, centerline velocities and temperature, local and average Nusselt numbers, etc.) are presented and discussed herein the ensuing section. The numerical results are also presented in the form of the predictive closure relationship.

Prior to the presentation of new results, the reliability and accuracy of the in-house computational flow solver is ascertained in the preceding sections by conducting the grid independence test, verification of the incompressibility limit (mandatory for LBM simulation) and comparison of the limiting results with the available literature.

Table 1. Grid independence test based on the average Nusselt number ($\overline{Nu}$) of a partially heated wall in the middle heating location by using the six dierent grids (G_1 to G_6) of uniform square lattice size ($N_x \times N_y$) at Ra=10^4 and Pr=0.7

Grid ($N_x \times N_y$)	$\overline{Nu}$	Number of iterations
G_1 (41×41)	2.881	16421
G_2 (61×61)	2.902	25023
G_3 (81×81)	2.915	34735
G_4 (101×101)	2.922	43048
G_5 (121×121)	2.931	53313
G_6 (521×521)	2.938	268547

1. Choice of Computational Parameters

The reliability and accuracy of any numerical solution procedure in CFD studies is naturally dependent upon a judicious choice of optimal parameters such as sizes of the computational domain and computational grid. In this work, the size of the computational domain, i.e., square, is itself fixed by the problem definition. In order to ensure the accuracy and reliability of present code and to determine the optimum lattice size, the grid independence study is carried out by using the six uniform grid lattice size ($N_x \times N_y$): G_1 (41×41), G_2 (61×61), G_3 (81×81), G_4 (101×101), G_5 (121×121) and G_6 (521×521). Here, N_x and N_y represents the number of lattice nodes in x- and y-directions, respectively. Table 1 shows the influence of grid lattice size on the average Nusselt number ($\overline{Nu}$) of a partially heated wall (x^*=0) with middle heating location at the fixed values of the Rayleigh (Ra=10^4) and Prandtl (Pr=0.7) numbers. An examination of grid independence study (Table 1) reveals that the refinement in the grid size from G_1 to G_6 relatively alters the value of the average Nusselt number ($\overline{Nu}$) by approximately 1.9%. The relative changes in the values of $\overline{Nu}$ due to the refinement of grid sizes $G_1 \rightarrow G_2$, $G_2 \rightarrow G_3$, $G_3 \rightarrow G_4$, $G_4 \rightarrow G_5$ and $G_5 \rightarrow G_6$ are seen to be of about 0.72%, 0.45%, 0.21%, 0.34% and 0.23% respectively. The above analysis of Table 1 shows marginal change in the average Nusselt number ($\overline{Nu}$) values on the further refinement of lattice grid size G_4, however, with the immense increase in CPU time to obtain the converged solution (as indicated by number of iterations to acquire the desired convergence when the solution started with similar initial guess values for each cases). Thus, the lattice grid size G_4 (101×101) is believed to be sufficiently refined enough to resolve the thermal and hydrodynamic features with an acceptable level of accuracy over the range of conditions considered herein. The results presented hereafter are based on the lattice grid size G_4 (101×101).

2. Quantification and Verification of Incompressibility Limit

The quantification of incompressibility limits is one of the necessity of the lattice Boltzmann method (LBM) solver a-prior to its utilization in the flow and thermal computations. Generally, the limits of compressibility/incompressibility are quantified in terms of the Mach number (Ma), which is defined [57] as

$$Ma = \frac{U}{c_s} \text{ where, the local speed of sound } c_s = \frac{c}{\sqrt{3}}$$

In order to compute the incompressible flow, LBM solvers must have the restriction of lower Mach number (Ma). The available lit-

Table 2. Values of characteristic velocity (U) and Mach number (Ma) for the considered range of Rayleigh number (Ra) at Pr= 0.71

Ra	U	Ma
10^3	0.007	0.012
10^4	0.030	0.050
10^5	0.100	0.170
10^6	0.170	0.290

erature [58] suggests that the Mach number value should be within permissible limit (i.e., Ma≤0.3) to maintain the condition of incompressible flow in the LBM solvers. Table 2 shows the values of characteristic velocity (U, Eq. (16)) and corresponding values of the Mach number (Ma). Over the range of Rayleigh number (Ra) considered herein, it can be observed that estimated values of the Mach number (Ma) are much less than the permissible limit (i.e., Ma<0.3 as incompressible limit). Therefore, the present PS-TLBM based numerical solution methodology is working well within the incompressible range. Hence, the present methodology is further confidently used to obtain the new results over the ranges of conditions considered herein.

3. Validation of Results

The analysis of the available literature suggests that none of the results are documented for the problem considered herein. However, considerable results are reported in the literature for the limiting case of the present problem, i.e., natural convection in an open ended square cavity comprising of the completely (L_h=1) heated isothermal left (x=0) wall and right (x=L) wall open to ambient conditions with thermally isolated top and bottom walls. To ascertain the reliability and accuracy of the present solution approach, therefore, the results obtained herein for the limiting case have been compared with the previous studies [34,39]. Table 3 compares the present values of the average Nusselt number ($\overline{Nu}$) of the completely (L_h=1) heated isothermal left (x=0) wall with the previous results [34,39] for the two values of the Rayleigh number ($Ra=10^4$ and 10^5) at a fixed value of the Prandtl number (Pr=0.7). An examination of Table 3 shows the maximum deviation of 1.96% in between the present results and literature values. The average deviation of the two (present and literature) values is seen to be about 0.6%. Such minor inherent errors tend to arise due to the enormous factors such as numerical methodologies, grid size, convergence criterion, approximations errors (round up and programming), etc [45, 49-52,59-66]. Keeping in mind the above mentioned inadvertent factors influencing the numerical results, the above comparison ascertains the confidence in the accuracy and reliability of the present in-house PS-TLBM solver. The results presented herein this work are, therefore, believed to be accurate and reliable within ±1-2%.

Table 3. Comparison of present numerical values of the average Nusselt number ($\overline{Nu}$) of completed heated isothermal left wall of open ended square cavity with the available literature at Pr=0.71

Source	$Ra=10^4$	$Ra=10^5$	$Ra=10^6$
Present	3.376	7.295	14.358
Mohamad et al. [34]	3.373	7.323	14.380
Kefayati [39]	3.319	7.391	14.404

Having gained the confidence in the present computational solution algorithm of PS-TLBM solver, the ensuing section presents the new results emphasizing the influence of flow governing parameters (i.e., heating location and Rayleigh number) on the detailed natural convection flow phenomenon of partially heated open cavity in terms of the streamline and isotherm patterns, center line variations of the velocity components and temperature, and local and average Nusselt numbers.

4. Detailed Convection Characteristics

The effect of heating location on local flow and thermal fields is examined through the contour profiles of the streamline, vorticity and temperature isotherms. The centerline variations of the velocity components and temperature are also examined to obtain the further insights into the nature of the flow. The kinematic viscosity (ν) and thermal diusivity (α) are the two significant fluid properties which are evidently responsible for the development of hydrodynamic and thermal boundary layers, respectively. The development of the boundary layers, in turn, influences the flow and heat transfer characteristics. Such influences are examined by systematic variation of the Rayleigh number (Ra), which is directly related to thickness of boundary layer. In order to delineate the influences of the flow governing parameters on the local field, the flow variables (Φ) is normalized as follow: $\Phi^*=(\Phi-\Phi_{min})/(\Phi_{max}-\Phi_{min})$, where Φ_{min} and Φ_{max} are the minimum and maximum values of the flow variable (Φ) in the computational domain under otherwise identical conditions.

Figs. 2-4 depict the representative dependence of the flow variables Φ^* (streamline ψ^*, vorticity ζ^* and temperature T^* isotherms) patterns on the heating locations and Rayleigh number (Ra) for the fixed length of heating (L_h=0.5) of the left wall. For the direct comparison purpose, the flow patterns (streamline, vorticity and isothermal contours) of cavity with completely heated (L_h=1) isothermal wall are included in the Figs. 2-4. Each figure consists of 21 equidistant contours ($\Delta\Phi^*$=0.05) of flow variables (ψ^*, ζ^* and T^*). In case of the complete heating of the left wall at $Ra=10^4$ (Fig. 2(d)), the flow is seen to enter from the lower half of open end of cavity, draw near heated wall resulting in rise in temperature which causes fluid to move in upward direction due to the buoyancy effect. During this motion of fluid, a gradual rise in temperature is observed from bottom (adiabatic) wall to the vicinity of top (adiabatic) wall of open end cavity. The fluid then starts approaching towards open end of cavity with gradual decrease in temperature. This clockwise movement of fluid causes formation of elliptical quasi-motionless portion in center of cavity with face opening towards the open end. This zone is created because of the variation in the density due to the change in temperature within the cavity. The isotherm patterns are slightly shifted towards heated part of cavity. This physical description of local flow patterns is in accordance with the literature [34,35,38].

For open ended cavity with partial heater (Fig. 2(a)-(c)), the flow and thermal patterns remain nearly same, except the isotherms are observed to be more stratified (dense crowding of isotherms) towards partially heated part due to the induced buoyancy eect. For

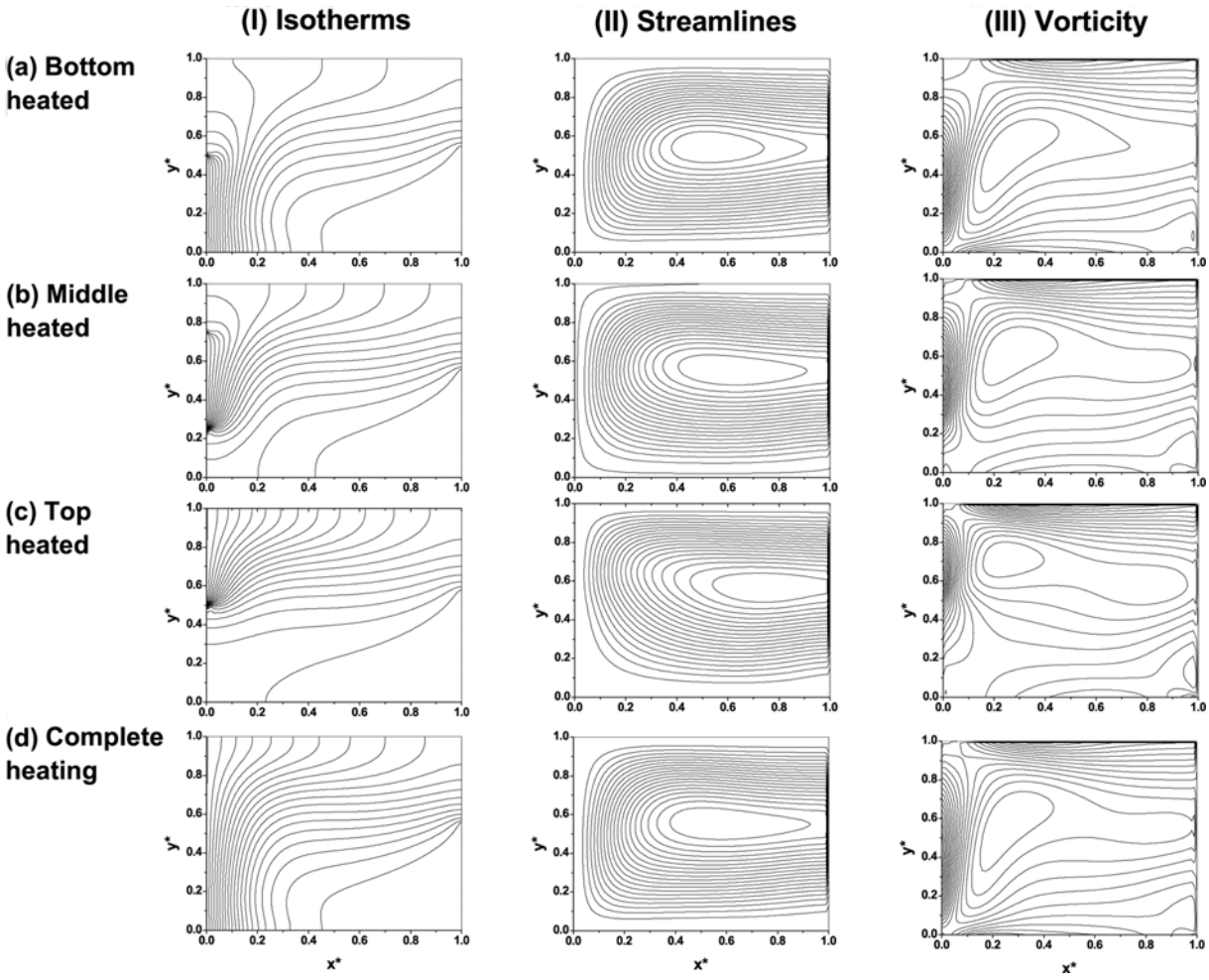

Fig. 2. Influence of heating locations of partially heated cavity on the isotherms, stream-function and vorticity contours at Rayleigh number of Ra=10^4. Patterns of completely heated open ended cavity are also included.

the bottom heated location, the flow entering from an open end approaches the heating surface, resulting in the rise in temperature. Subsequently, the heated fluid moves upward due to the induced buoyancy effect and reaches the adiabatic part of the partially heated wall. Further, fluid flows toward the open end of cavity with decrease in the fluid temperature. For all the three heating locations (Fig. 2(a)-(c)), streamline patterns remain qualitatively similar. However, the size of elliptical quasi-motionless region (or convection cell) is seen to be smallest for the bottom heating and largest for the middle heating location. The zone of recirculation shifts from the center towards the open end with the change in heating location from bottom to middle and then to the top, respectively. It is observed that due to increase in the heat source intensity (Rayleigh number), the strength of these convection cell increases, which is evident from increase in the size of these cell with Ra. The vorticity contours (Fig. 2III) show the vortex formation near the partially heated wall. It is clearly due the sharp changes in the temperature of fluid in the vicinity of the heated section of the cavity.

With an increase in Rayleigh number (Ra), the isotherms become more concentrated towards heating location (i.e., dense clustering of constant temperature lines toward the heated part) and, in case of top and middle heating locations, the lower half of domain becomes nearly isothermal (refer Fig. 3). This may be due to increase in Ra, causing increase in flow penetration capacity of fluid. These patterns are also seen to be consistent with the available literature on the completely heated open ended cavity [38]. This is undoubtedly due to increasing buoyancy effect with increasing Ra, i.e., the increase in Rayleigh number (heat intensity) increases fluid movement in the cavity between hot wall to ambient (open end). It causes change in shape and size of the re-circulation zone formed in the center of cavity for three dierent heating locations. The formation of vortex (or convection cell) is also observed at the bottom corner of the open end of cavity. The size of vortex is seen to vary with the change in the heating location. For instance, top heating has larger vortex structure than other two cases. It is due to the fact that flow is expected to enter from lower half of open end wall, whereas the region close to bottom part of open end wall is unable to approach towards heated surface due to the weak buoyancy effect. It, in turn, forms the cavity with bottom heating has minimum vortex size then followed by middle heating cavity. Moreover, the increase in Ra, decreases the thermal boundary layer thickness, which can be observed from the isotherm figures (Figs. 2-4).

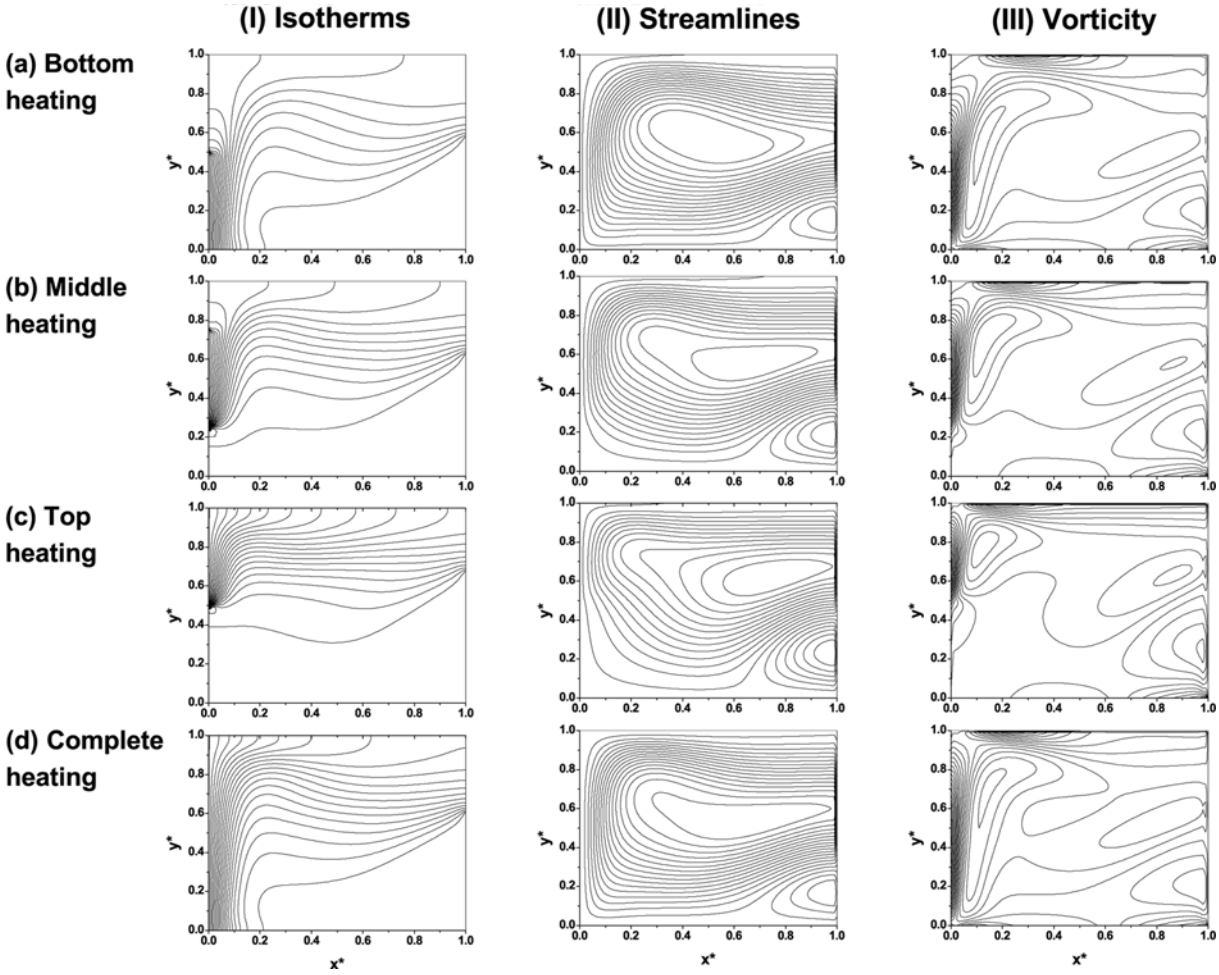

Fig. 3. Influence of heating locations of partially heated cavity on the isotherms, stream-function and vorticity contours at Rayleigh number of Ra=10^5. Patterns of completely heated open ended cavity are also included.

On further increase in the Rayleigh number to Ra=10^6 (Fig. 4), the fluid movement between heated and open boundaries increases due to strengthening of the buoyancy effect. The temperature isotherms become much more stratified with dense clustering of isotherm lines towards partially heated wall, which implies higher rate of heat transfer. In the center of cavity, the isotherms becomes almost parallel to horizontal axis. It is due to increase in size of quasi-motionless region in the center of cavity, which can be seen from the streamline patterns. Due to the increased fluid circulation, elliptical motionless region breaks into two vortices. The size of vortex is found to vary with the change in heating location due to the variable magnitude of buoyancy force. It is evident from isotherms, that for top heating location, the isotherms are distributed in upper top half of cavity, as for this location, the fluid circulation remains active along top half of cavity, with lower half of cavity remains stagnant.

Further insights of the local flow patterns are gained by analyzing the variations of the temperature and velocity components along the geometric centerlines. Fig. 5 represents the variation of temperature along both horizontal and vertical centerlines of the cavity, i.e., $T^*(y^*)$ at $x^*=0.5$ and $T^*(x^*)$ at $y^*=0.5$, respectively, for the partial (L_h=0.5) isothermal heating at three different heating locations on the cavity wall as well as for the complete (L_h=1) isothermal heated wall. Irrespective of the governing parameters (i.e., heating length/location and Ra), the dimensionless temperature (T^*) is observed to gradually increase (Fig. 5I) from its minimum value ($T^*\approx 0$ at $y^*=0$) to a maximum value with increase in y^* along the horizontal centerline ($x^*=0.5$). The variation of temperature in the bottom region of the cavity (i.e., $y^*\lesssim 0.3$) is insignificant. However, a sharp increase in the temperature with increase in y^* is seen above the initial region (i.e., $0.3\lesssim y^*\lesssim 0.9$). The maximum temperature remains nearly constant in the region close to the top wall (i.e., $0.9\lesssim y^*\leq 1$). The shifting of partial heating location (from bottom to middle and then to top) shows a significant variation in the temperature in the second region (i.e., $0.3\lesssim y^*\lesssim 0.9$). Irrespective of the value of Ra, the maximum value of the temperature in the close vicinity of top wall (i.e., $0.9\lesssim y^*\leq 1$) is seen to decrease with shifting of partial heating location from bottom to middle and then to top, respectively. The partial heating at bottom and complete isothermal heating shows qualitatively as well quantitatively similar temperature distribution along the horizontal centerline. In case of the top heating, the heat is lost during motion of fluid from entry towards top heated wall due to a linear increase in temperature along vertical line. Moreover, the maximum temperature remains same ($T^*_{max}\approx 0.65$) for middle and top heating whereas $T^*_{max}\approx 0.45$ for bottom

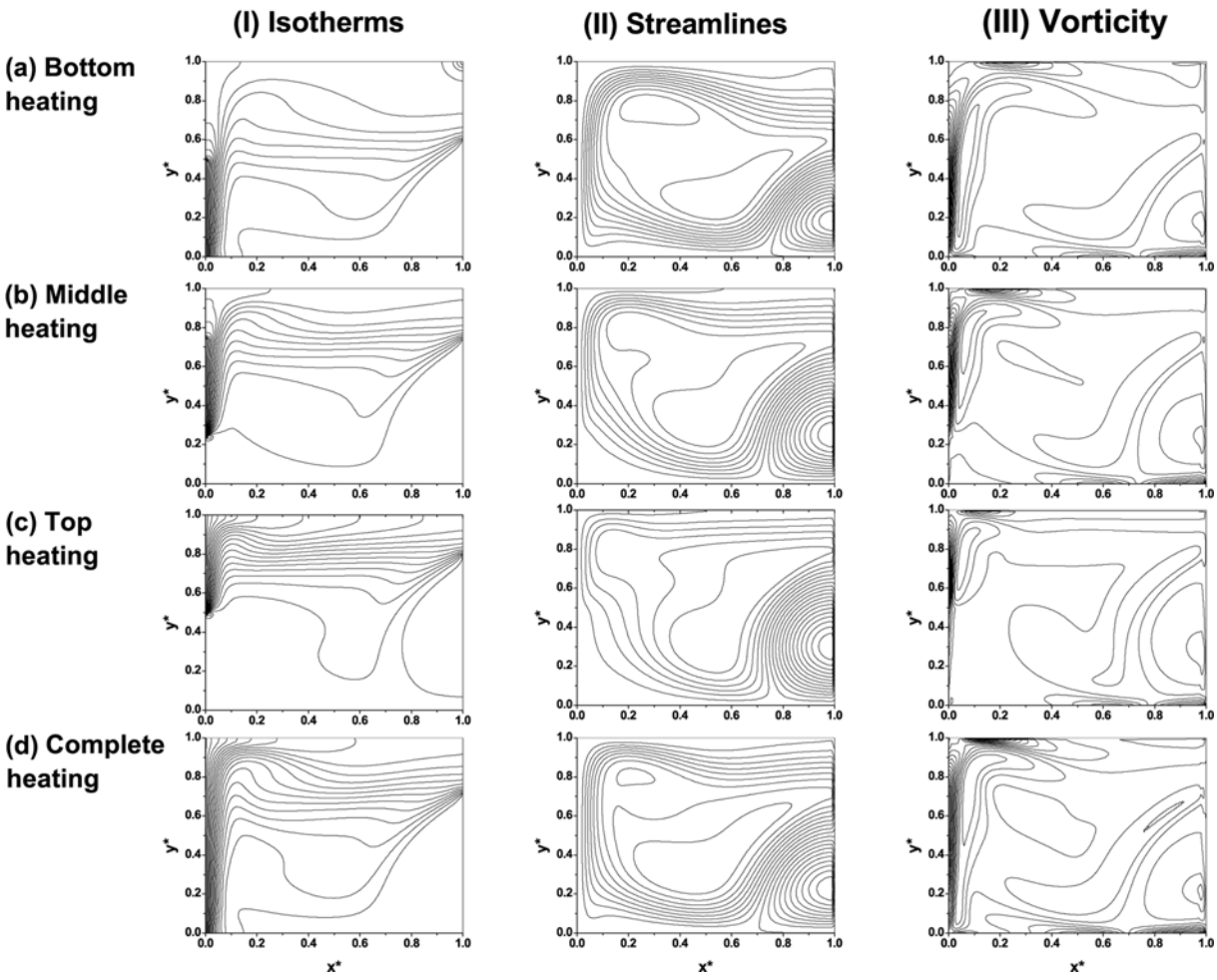

Fig. 4. Influence of heating locations of partially heated cavity on the isotherms, stream-function and vorticity contours at Rayleigh number of Ra=10^6. Patterns of completely heated open ended cavity are also included.

heating.

On the other hand, the temperature (T^*) is seen to gradually decrease (Fig. 5II) from its maximum value ($TT^*_{max}\approx1$ at $x^*=0$) to a minimum value ($T^*\approx0$ at $x^*=1$) with increase in x^* along the vertical centerline ($y^*=0.5$). In case of the partial heating, cavity with middle heating has higher maximum temperature ($T^*_{max}\approx1.0$) compared to the other two heating locations, where the maximum temperature is $T^*_{max}<1.0$. A sudden drop in the temperature (T^*) is clearly visible near the heated left wall of the cavity for all the values of Ra and heating locations. The decrease in the temperature along the horizontal axis (x^*) is due to the clock-wise induced buoyancy flow. It is interesting to note from the temperature curves (T^* vs x^*) that, irrespective of the heating arrangements, the temperature (T^*) drops to zero (i) at the open end of the cavity ($x^*\approx1$) for the lower values of the Rayleigh number ($Ra\leq10^5$), and (ii) within the cavity ($x^*<1$) for higher values of the Rayleigh number ($Ra>10^5$). The shifting of the zero temperature ($T^*=0$) position on the vertical centerline is seen to be maximum (≈15-20%) and minimum (≈5%) within the cavity for the top and bottom heating locations, respectively. Such a shift of the zero temperature position suggests the enlargement (or contraction) of effective convection zone within the cavity.

Consequent variations of the horizontal and vertical velocity components (i.e., u^*_x and u^*_y) along the vertical and horizontal centerlines (i.e., $x^*=0.5$ and $y^*=0.5$), respectively, are illustrated in Fig. 6 for the range of Rayleigh number (Ra) and heating size/locations. Irrespective of the governing conditions, the circulation of fluid due to the induced buoyancy is clearly evident from Fig. 6. The amplitude of the fluid circulation is also seen to be strongly dependent on both the Rayleigh number (Ra) and the heating size/locations. The horizontal velocity profiles (u^*_x vs y^*) have similar values (i.e., zero, see Fig. 6I) at both the ends ($y^*=0$ and 1) due to the no-slip solid (bottom and top) stationary walls of the cavity. In general, the horizontal velocity profiles (u^*_x vs y^*) originate from zero at $y^*=0$ and attains its minimum (and negative) value. It is followed by the gradual increase until it reaches to a maximum (and positive) value. It, further, drops down to the zero value along the vertical centerline. Therefore, it represents the buoyancy induced circulatory flow in between the walls ($0<y^*<1$) through the appearance of both the negative and positive values of the velocity (u^*_x) in the lower and upper half sections of the cavity. The symmetrical amplitude of flow circulation deviates with change in heating from complete to partial isothermal heating for all values of the Rayleigh number. The intensity of recirculation also enhances with increas-

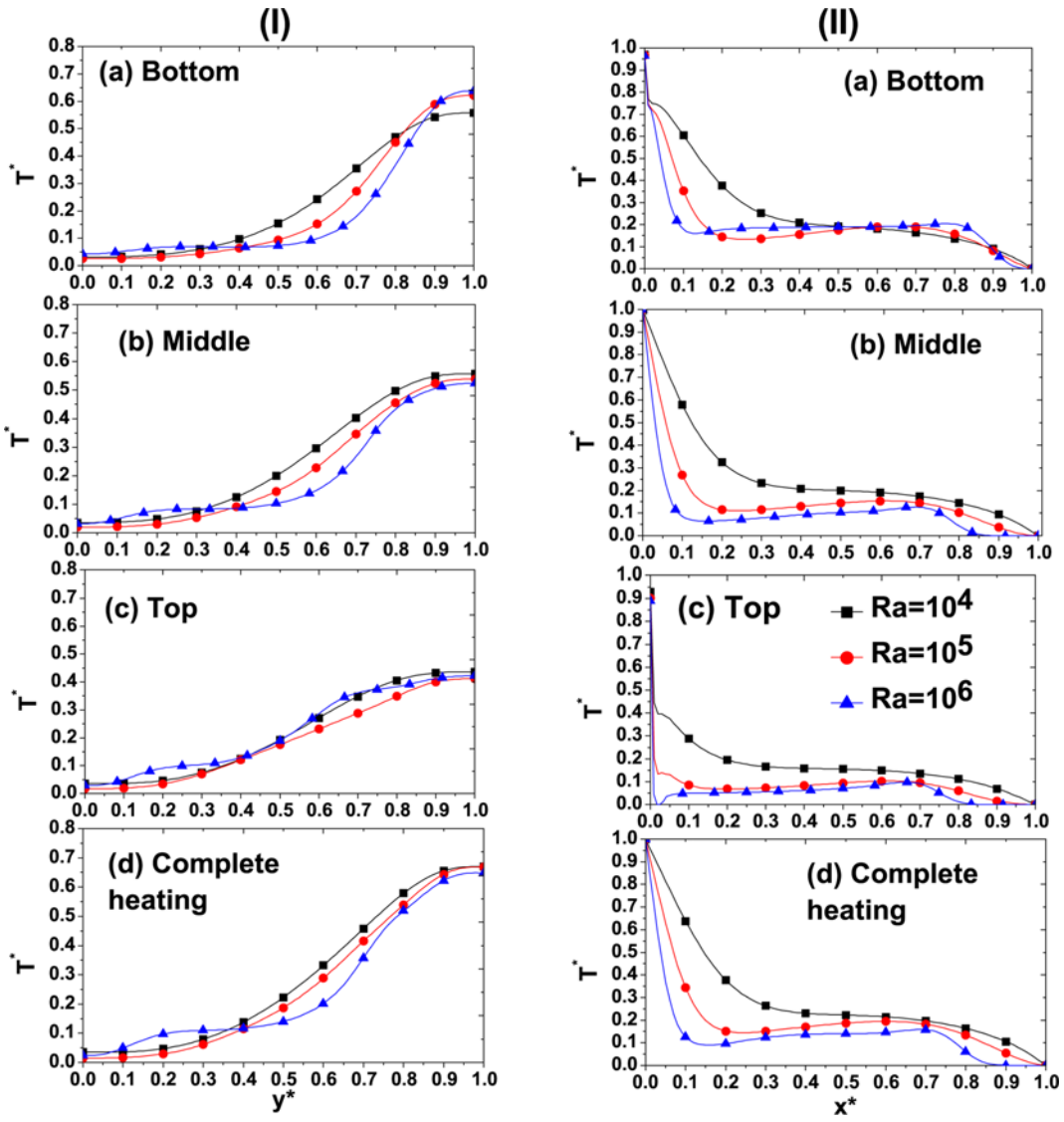

Fig. 5. Dimensionless temperature (T^*) variation along (I) vertical (x^*=0.5) and (II) horizontal (y^*=0.5) centerlines of cavity with Rayleigh number ($10^4 \le Ra \le 10^6$), partial heating at different locations and complete heating.

ing value of the Rayleigh number (Ra) for all the heating locations. Similarly, the distributions of the vertical velocity (u_y^* vs x^*) along the horizontal centerline (y^*=0.5) of cavity are depicted in Fig. 6(II). Similar to the horizontal velocity profiles (u_x^*), the vertical velocity patterns (u_y^*) also show a complex dependence on the flow governing parameters. It shows that the zero velocity at the no-slip solid stationary left wall increases sharply to its maximum value and then a gradual decrease in the values near the open end of the cavity. The velocity profiles are nearly unchanged in the middle portion of cavity. However, the sharp decrease to the minimum value followed by an increase to zero or finite value in the close vicinity of the right open end wall is observed. At lower values of the Rayleigh number ($Ra \le 10^5$), the vertical velocity (u_y^*) is seen to have zero value for all the heating situations. However, finite value of vertical velocity (u_y^*) can be seen for the higher values of Rayleigh number ($Ra > 10^5$). These are the articulated fact (Fig. 6II) arising due to interesting feature observed in the centerline temperature distribution curves (Fig. 5II). It can also be observed from Fig. 6 that the influences of flow governing parameters is more predominant on the horizontal velocity profiles (u_x^* vs y^*) compared to that on the vertical velocity (u_y^* vs x^*).

The detailed flow and thermal characteristics, presented and discussed in foregoing section, are seen to have complex dependence on the natural convection flow governing parameters. These, in turn, will alter the global convection characteristic, such as local and average Nusselt number, etc. Therefore, the functional dependencies of local and averaged heat transfer rate on the flow governing parameters are explored in the ensuing section.

5. Global Convection Characteristics

The Nusselt number (or dimensionless heat transfer coefficient) is generally considered as one of the important engineering parameter to signify the rate of convective heat transfer. In this section, the functional dependence of local (as well as average) Nusselt number on the flow governing parameters is presented and discussed for

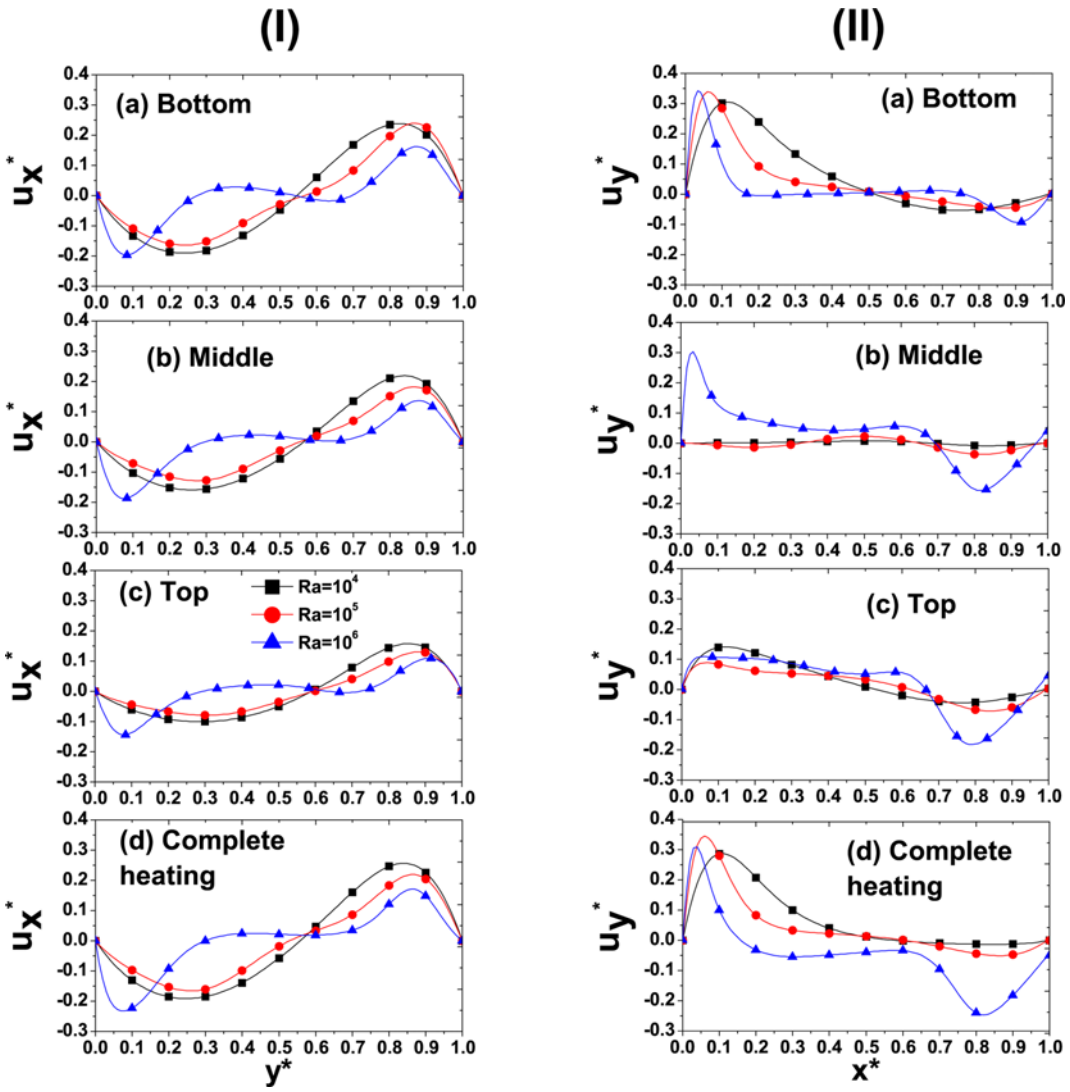

Fig. 6. Variations of (I) horizontal component of velocity (u^*_x) along the vertical (x^*=0.5) and (II) vertical component of velocity (u^*_y) along the horizontal (y^*=0.5) centerlines of cavity with Rayleigh number ($10^4 \le Ra \le 10^6$), partial heating at dierent locations and complete heating.

the wide range of Rayleigh number ($10^3 \le Ra \le 10^6$), partial/complete ($L_{ii} \le 1$) isothermal heating and heating locations of the open ended cavity.

Fig. 7 depicts the local Nusselt number (Nu, Eq. (19)) distribution on the partially heated left wall (x^*=0, y^*) over the ranges of conditions considered herein. Irrespective of the heating size and location, as expected, the local Nusselt number (Nu) is found to increase with increasing value of Rayleigh number (Ra). For all the cases considered herein, the local Nusselt number decreased along the length of heating ($h^*_1 \le y^* \le h^*_2$, refer Eq. (12)) of the wall, under otherwise identical conditions. The sharp peaks can also be observed in Fig. 7 at the starting (of the middle and top heating locations) and at the end (of bottom and middle heating locations), respectively. Such peaks represent the sharp changes in thermal gradients at those spatial locations due to the sudden change in the heating mode from isothermal to adiabatic and vice versa. The sharp gradients ultimately leads to the higher heat transfer at such local locations. The peaks, if observed, are always higher at the starting point, compared to that at the end point, of the heating location because of the larger (and sudden) temperature variations at this location. Irrespective of the value of Rayleigh number (Ra), the smaller peaks observed in the local Nusselt number curves (Figs. 7(a) & 7(b)) represent the change of the heating mode from isothermal to adiabatic and vice versa (from adiabatic to isothermal) is seen through larger peaks in the Nu curves (Figs. 7(b) & 7(c)). For the fixed value of Ra, a single peak in Nu curve is noticed in case of both the bottom and top heating (Figs. 7(a) & 7(c)) arrangements while two peaks appeared in the middle heating (Fig. 7(b)) case. The appearance of peaks in these curves suggests the local enhancement of the heat transfer. The occurrence of the two (one smaller and one larger) peaks in the middle heating case (Fig. 7(b)), thereby, represents the maximum heat transfer amongst other heating cases for the fixed value of Rayleigh number. For the lowest considered Rayleigh number ($Ra=10^4$), the Nusselt number varies in

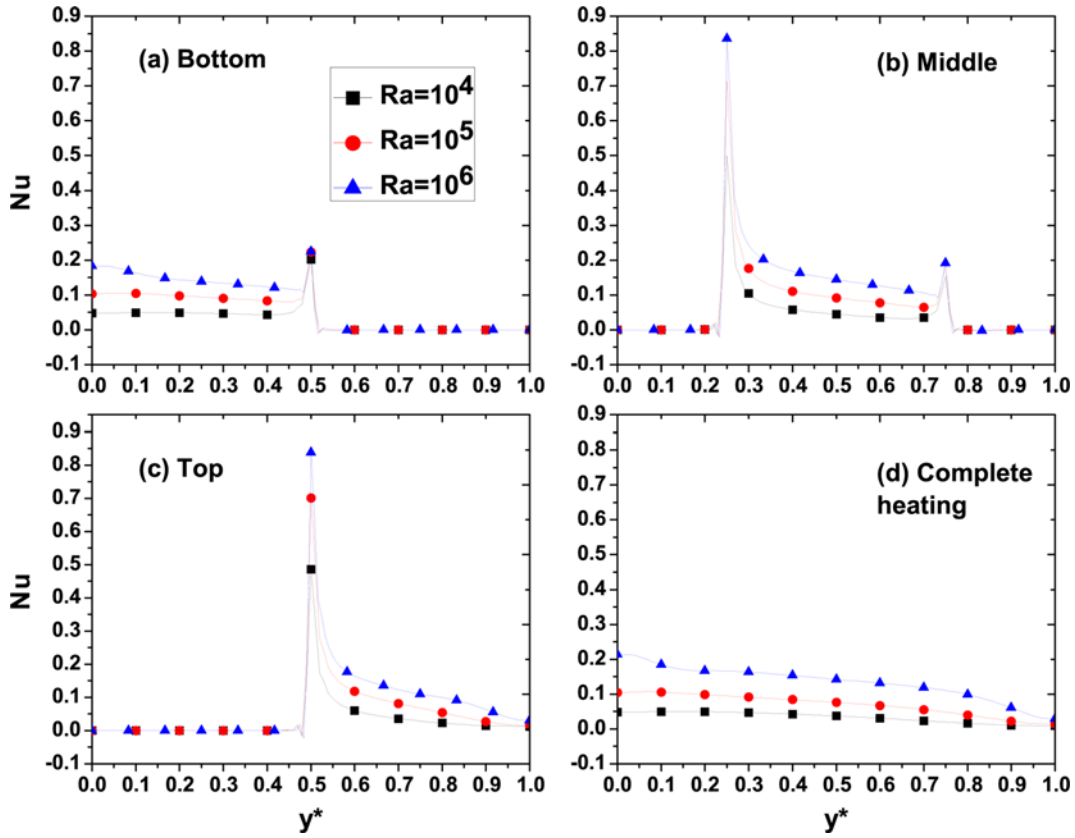

Fig. 7. Dependence of the local Nusselt number (Nu) of the hot wall (x^*=0) on the heating locations and Rayleigh number ($10^4 \le Ra \le 10^6$).

the range of 0.05-0.1 for all the three heating conditions, thereby, implying the weak convection and low rate of heat transfer. The Nusselt number values increased up to 0.1-0.25, with increasing Ra, suggesting an increased heat transfer rate. Such heat transfer patterns can clearly by identified from the isotherm patterns. At low Rayleigh number, isotherms distribution is thin with thick thermal boundary layer indicating low rate of heat transfer. With the increase in Rayleigh number, thermal boundary layer becomes thin with dense and stratified isotherms along hot wall which implies higher rate of heat transfer.

Further, the average Nusselt number ($\overline{Nu}$, Eq. (20)) is obtained by integrating the local Nusselt number (Nu) values over the heated wall. Table 4 presents the dependence of the average Nusselt number ($\overline{Nu}$) on the Rayleigh number ($10^3 \le Ra \le 10^6$), heating size ($L_h \le 1$) and three different (bottom, middle and top) heating locations on the active wall. Irrespective of the heating arrangements, the average Nusselt number ($\overline{Nu}$) is seen to increase in the unambiguous manner with an increasing value of the Rayleigh number (Ra). As

Table 4. Dependence of the average Nusselt number ($\overline{Nu}$) on the heating location and Rayleigh numbers

Heating position	L_h	Ra=10^3	Ra=10^4	Ra=10^5	Ra=10^6
Top	0.5	1.485	2.053	4.019	7.161
Middle	0.5	2.031	2.921	5.385	9.308
Bottom	0.5	1.655	2.494	4.786	8.895
Complete heating	1.0	1.387	3.376	7.295	14.358

noted in the local Nusselt number (Nu) variations, the middle heating case yields the largest value of the average Nusselt number ($\overline{Nu}$), followed by the bottom and top heating arrangements. Furthermore, a comparison of partial heating (L_h<1) arrangements with the complete heating (L_h=1) suggests that for the equal size of heating, the partial heating arrangements enhance the average heat transfer in the open ended cavity.

To delineate the role of partial heating (L_h<1) over the complete heating (L_h=1) on the average heat transfer in the open ended square cavity, the average Nusselt number values have been normalized with the corresponding values of complete heating, under otherwise identical conditions. The normalized Nusselt number (Nu^N) is expressed as follows:

$$Nu^N = \frac{\overline{Nu}_{(L_h<1)}}{\overline{Nu}_{(L_h=1)}} \tag{40}$$

Fig. 8 represents the variation of normalized average Nusselt number (Nu^N) with the Rayleigh number ($10^3 \le Ra \le 10^6$) for the different heating locations. Irrespective of the heating locations, qualitatively similar dependence of Nu^N on Ra is observed over the ranges of conditions considered herein. It is clearly evident from Fig. 8 that open ended square cavity with middle heating arrangement have higher rate of heat transfer than the bottom followed by top heating configurations. The normalized values above and lower than unity (i.e., Nu^N>1 and Nu^N<1) suggest the enhancement and deterioration in the heat transfer in comparison to the completely heated open ended cavity. The difference of the heating lengths in both

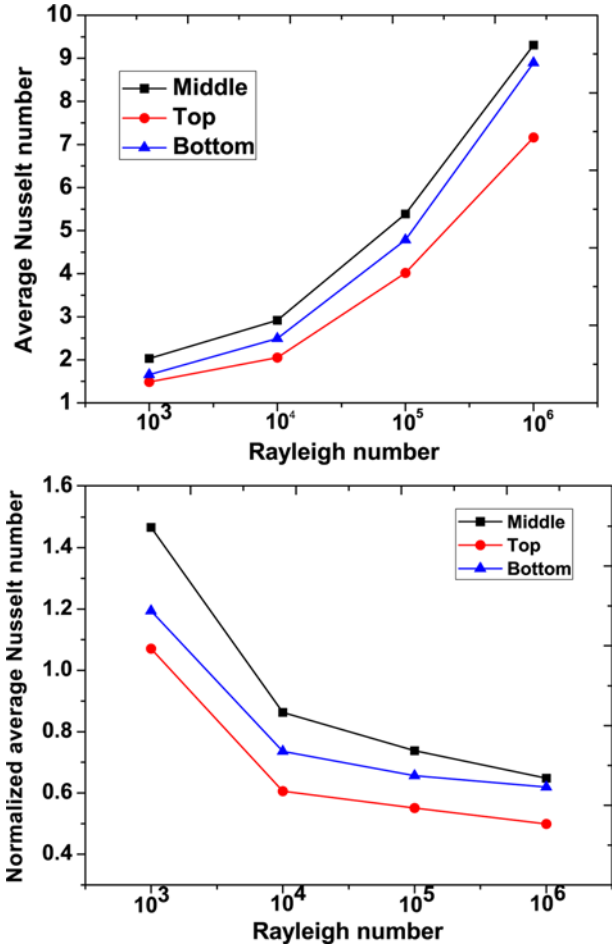

Fig. 8. Dependence of the average Nusselt number (Nu) of the hot wall ($x^*=0$) on the heating locations and Rayleigh number ($10^3 \le Ra \le 10^6$).

partial and complete heating arrangements should also be noted a-prior to the analysis of Fig. 8. The half (H/2) of cavity wall is exposed to heating in case of the partial isothermal heating arrangements in comparison to the whole length (H) is heated in complete heating. Therefore, for the equal size of heating in both the partial and complete heating arrangements, the partial heating at any of location enhances the average heat transfer in the open ended cavity.

Further attempts are also made to establish the functional relationship between the flow governing parameters and the average Nusselt number. The subsequent discussion presents an empirical predictive correlation of average Nusselt number.

5-1. Empirical Correlation

The development of a simple predictive correlation is essential in order to obtain the dependent variable for the intermediate values of the independent variables for their best possible utilization in engineering practices and design. Considering an important aspect from an engineering and scientific point of view, therefore, attempts are made to develop an empirical correlation elucidating the functional dependence of the present numerical values of the average Nusselt number ($\overline{Nu}$) on the flow governing parameters. In order to get best fit correlation, the functional dependence of the average Nusselt number ($\overline{Nu}$) on the Rayleigh number (Ra)

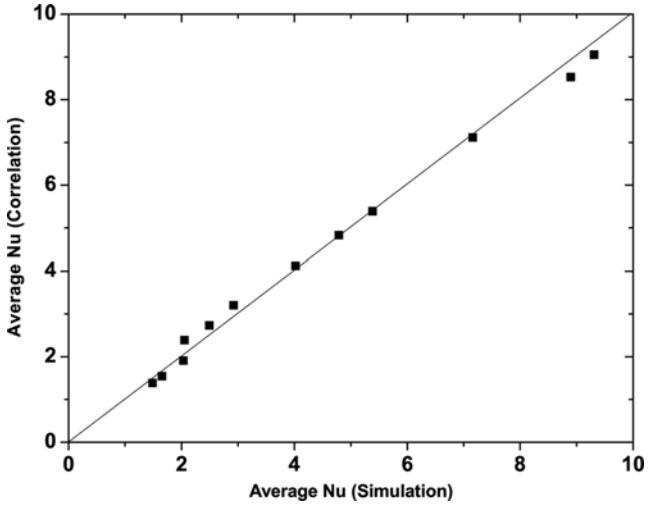

Fig. 9. Comparison of present numerical and predicted (Eq. (41)) average Nusselt numbers.

for different heating length/locations is represented by the following power-law expression (as most of the heat transfer correlations are expressed as power-law function [67]).

$$\overline{Nu}=ARa^{B} \tag{41}$$

The statistical analysis of the present numerical data yields the correlation coefficients (A and B in Eq. (41)) as,

$$A=-2.054L_{hc}^2+2.031L_{hc}-0.099;\ B=0.260L_{hc}^2-0.290L_{hc}+0.303 \tag{42}$$

with an excellent coefficient of determination ($R^2=0.98$) over the investigated ranges of conditions ($10^4 \le Ra \le 10^6$ and $0.25 \le L_{hc} \le 0.75$). Here, L_{hc} being the center of heating location encompassing the heating length. It can be mathematically described as the summation of the initial point of heater (h_o or y_1 or y_1^* refer Eq. (5) or (12)) and center of uniform heating ($l_h/2$ or $L_h/2$) of partial heater. It can be expressed as follows:

$$l_{hc}=h_o+\frac{l_h}{2} \quad \text{or} \quad L_{hc}=y_1^*+\frac{L_h}{2} \tag{43}$$

For the equal size of isothermal heating (i.e., $L_h=1/2$) at all the heating locations, the value of L_{hc} of 1/4, 1/2 and 3/4 corresponds to the bottom, middle and top heating location, respectively, in the development of the above empirical correction (Eq. (41)).

Furthermore, the present numerical values and the predicted values (Eq. (41)) of the average Nusselt number ($\overline{Nu}$) shows a maximum and average deviation of 13.5% 1.07%, respectively. Fig. 8 represents the best fit between the two (numerical and empirical) values of average Nusselt number ($\overline{Nu}$). It should also be noted that maximum deviations between two values is seen to be in the order of ±3-4% for all the conditions, except that of ~13.5% at the Rayleigh number of $Ra=10^4$ for top heating location ($L_{hc}=0.75$). Excluding this point the maximum deviation is observed to be 9.2% for bottom heating and $Ra=10^3$. It is observed that the proposed predictive closure correlation (Eq. (41)) predicts the average Nusselt number ($\overline{Nu}$) values within acceptable level of deviations from the computed values.

CONCLUDING REMARKS

The natural convection in the partially heated open ended square cavity has been numerically investigated by using the in-house developed (in C++) computational flow solver based on the passive scalar thermal lattice Boltzmann method (PS-TLBM) with *D2Q9* lattice model. The partial part of the left wall of the cavity is isothermally heated at either of the three different (bottom, middle and top) heating locations. The remaining part of left wall, top and bottom walls are maintained adiabatically. The right end of the cavity is open to ambient conditions. The local and global flow characteristics such as streamline, isotherm and vorticity patterns, centerline variations of the velocity components and temperature, local and average Nusselt number have been presented and discussed. The present results can be concluded as follow: At low Rayleigh number (Ra= 10^4), streamline patterns remain qualitatively similar for all the three heating location. However, the size of the re-circulation zone changes with the shifting of heating locations. The largest recirculation zone is observed for the middle heating case. The isotherm patterns are shifted towards the partially heated wall. With an increase in the Rayleigh number (Ra=10^5), the streamline patterns shows clockwise circulation with formation of vortex near lower part of open end of cavity. The top heating yielded the maximum size of vortex. On further increase in the Rayleigh number (Ra=10^6), the elliptical quasi motionless region breaks in two vortices which take shape according to position of heating location. Both the local and average Nusselt numbers have shown the linear dependence on the Rayleigh number for all the three partial heating cases. Finally, the functional dependence of present numerical results of average Nusselt number ($\overline{Nu}$) on the Rayleigh number (Ra) and heater location (L_{hc}) have also been presented as a simple closure empirical relationship. Irrespective of the value of the Rayleigh number, cavity with middle partial heating location shown higher average Nusselt number (or heat transfer rate) followed by bottom and top heating location, respectively.

REFERENCES

1. R. Jmai, B. Ben-beya and T. Lili, *Superlattices and Microstructures*, **53**, 130 (2013).
2. K. M. Gangawane, R. P. Bharti and S. Kumar, Thermal lattice Boltzmann methods: a review, in: Conference on Technological Advancements in Chemical and Environmental Engineering (TACEE-2012), Paper no. O270, BITS Pilani, Pilani, India, March 23-24 (2012).
3. K. M. Gangawane, R. P. Bharti and S. Kumar, *Thermal analysis of natural convection in dierentially heated shallow cavities at dierent Rayleigh numbers by lattice Boltzmann approximation*, in: Proceedings of 65th Annual Session of IIChE (CHEMCON-2012), International Conference on Sustainable Technologies for Energy and Environment in Process Industries and Indo-US Joint International Conference on Energy and Environment, Paper no. P-311, NIT Jalandhar, Jalandhar, India, December 27-30 (2012).
4. K. M. Gangawane, R. P. Bharti and S. Kumar, *Lattice Boltzmann simulation of natural convection in a partially dierentially heated square enclosure*, in: Proceedings of the 22nd National and 11th ISHMT-ASME Heat and Mass Transfer Conference, Paper no. HMTC1300114, IIT Kharagpur, Kharagpur, India, December 28-31 (2013).
5. K. M. Gangawane, R. P. Bharti and S. Kumar, *Can. J. Chem. Eng.*, **93**(4), 766 (2015).
6. R. E. Spall, *Int. J. Heat and Mass Transfer*, **23**, 115 (1996).
7. E. Bilgen and A. Muftuoglu, *Int. Commun. Heat Mass Transfer*, **35**, 545 (2008).
8. T. H. Hsu and S. G. Wang, *Numerical Heat Transfter, Part A: Appl.*, **38**, 627 (2000).
9. S. Q. Du, E. Bilgen and P. Vasseur, *Int. J. Heat Mass Transfer*, **34**, 263 (1998).
10. K. L. Hsiao, *Appl. Therm. Eng.*, **27**, 1895 (2007).
11. S. Habib, C. Surry and A. Belghith, *High Temperature Material Process*, **9**, 483 (2005).
12. A. Hobbi and K. Siddiqui, *Int. J. Heat Mass Transfer*, **52**, 4650 (2009).
13. Y. A. Cengel and J. G. Afshin, Heat and Mass Transfer, McGraw Hill Higher Education, 2nd Ed. (2011).
14. A. Valencia and R. L. Frederick, *Int. J. Heat Mass Transfer*, **32**(8), 1567 (1989).
15. R. Begum and M. A. Basit, *European Journal of Scientific Research*, **22**, 216 (2008).
16. H. Xi, G. Peng and S. H. Chou, *Phys. Rev. E*, **59**, 6202 (1999).
17. Y. Dong, J. Zhang and G. Yan, *Applied Mathematical Modelling*, **34**, 481 (2010).
18. F. J. Alexander, S. Chen and J. D. Sterling, *Phys. Rev. E*, **47**, R2249 (1993).
19. X. He, S. Chen and G. D. Doolen, *J. Comput. Phys.*, **146**, 282 (1998).
20. Y. Peng, C. Shu and Y. Chew, *Phys. Rev. E*, **68**(2), 026701 (2003).
21. F. Kuznik, J. Vareilles, G. Rusaouen and G. Krauss, *Int. J. Heat Fluid Flow*, **28**, 862 (2007).
22. Z. Guo, C. Zheng, B. Shi and T. S. Zhao, *Phys. Rev. E*, **75**, 1 (2007).
23. S. Chen and Z. Tian, *Int. J. Heat Fluid Flow*, **31**, 227 (2010).
24. C. B. Shin and D. J. Economou, *Int. Commun. Heat Mass Transfer*, **33**(10), 2191 (1990).
25. K. Vafai and J. Ettefagh, *Int. Commun. Heat Mass Transfer*, **33**(10), 2329 (1990).
26. C. Balaji and S. P. Venkateshan, *Int. J. Heat Fluid Flow*, **15**(4), 317 (1994).
27. A. A. Mohamad, *Numerical Heat Transfter, Part A: Appl.*, **27**, 705 (1995).
28. D. Angirasa, J. G. M. Eggels and F. T. M. Nieuwstadt, *Numerical Heat Transfter, Part A: Appl.*, **28**, 755 (1995).
29. K. Khanafer and K. Vafai, *Int. J. Heat Mass Transfer*, **43**, 4087 (2000).
30. K. Khanafer and K. Vafai, *Int. J. Heat Mass Transfer*, **45**, 2527 (2002).
31. O. Polat and E. Bilgen, *Int. J. Therm. Sci.*, **41**, 360 (2002).
32. J. F. Hinojosa, R. E. Cabanillas, G. Alvarez and C. E. Estrada, *Int. Commun. Heat Mass Transfer*, **32**(9), 1184 (2005).
33. E. Bilgen and H. Oztop, *Int. J. Heat Mass Transfer*, **48**(8), 1470 (2005).
34. A. A. Mohamad, M. El-Ganaoui and R. Bennacer, *Int. J. Therm. Sci.*, **48**(10), 1870 (2009).
35. H. Sajjadi, M. Gorji, G. R. Kefayati, D. D. Ganji and M. Shayannia, *World Academy of Science, Engineering and Technology*, **55**, 265 (2010).
36. M. Prakash, S. B. Kedare and J. K. Nayak, *Int. J. Therm. Sci.*, **51**, 23 (2012).

37. S. Chung and K. Vafai, *Int. J. Heat Mass Transfer*, **53**, 2703 (2010).
38. A. Haghshenas, M. R. Nasr and M. H. Rahimian, *Int. J. Heat Mass Transfer*, **53**, 1513 (2010).
39. G. R. Kefayati, *Int. Commun. Heat Mass Transfer*, **40**, 67 (2013).
40. M. Sankar, M. Bhuvaneswari, S. Sivasankaran and Y. Do, *Int. J. Heat Mass Transfer*, **54**, 5173 (2011).
41. M. M. Rahman, H. F. Oztop, R. Saidur, S. Mekhilef and K. Al-Salem, *Comput. Fluids*, **79**, 53 (2013).
42. R. B. Bird, W. E. Stewart and E. N. Lightfoot, Transport Phenomena, John Wiley & Sons, Inc., 2nd Ed. (2006).
43. R. P. Chhabra and J. F. Richardson, Non-Newtonian Flow and Applied Rheology, Butterworth-Heinemann, Oxford, UK, 2nd Ed. (2008).
44. W. M. Deen, Analysis of Transport Phenomena, Oxford University Press, 2nd Ed. (2013).
45. A. T. Srinivas, R. P. Bharti and R. P. Chhabra, *Ind. Eng. Chem. Res.*, **48**, 9735 (2009).
46. A. Bejan, Convective Heat Transfer, John Wiley & Sons, Inc., 3rd Ed. (2004).
47. E. Fattahi, M. Farhadi and K. Sedighi, *Int. J. Therm. Sci.*, **49**, 2353 (2010).
48. E. Fattahi, M. Farhadi, K. Sedighi and H. Nemati, *Int. J. Therm. Sci.*, **52**, 137 (2012).
49. R. P. Bharti, R. P. Chhabra and V. Eswaran, *Heat Mass Transfer*, **43**(7), 639 (2007).
50. R. P. Bharti, R. P. Chhabra and V. Eswaran, *Int. J. Heat Mass Transfer*, **50**(5-6), 977 (2007).
51. R. P. Bharti, R. P. Chhabra and V. Eswaran, *Chem. Eng. Sci.*, **62**(7), 4729 (2007).
52. R. P. Bharti, P. Sivakumar and R. P. Chhabra, *Int. J. Heat Mass Transfer*, **51**(7-8), 1838 (2008).
53. Y. L. Chan and C. L. Tien, *Numerical Heat Transfter, Part A: Appl.*, **8**, 65 (1985).
54. S. Chen and G. D. Doolen, *Annual Reviews of Fluid Mechanics*, **30**, 329 (1998).
55. Y. Peng, C. Shu and Y. Chew, *J. Comput. Phys.*, **193**(1), 260 (2004).
56. Q. Zou and X. He, *Phys. Fluids*, **9**, 1591 (1997).
57. Y. He, C. Qi, Y. Hu, B. Qin, F. Li and Y. Ding, *Nanoscale Res. Lett.*, **6**, 1 (2011).
58. P. J. Dellar, *Nanoscale Res. Lett.*, **190**, 351 (2013).
59. R. P. Bharti, R. P. Chhabra and V. Eswaran, *Canadian J. Chem. Eng.*, **84**(4), 406 (2006).
60. P. Sivakumar, R. P. Bharti and R. P. Chhabra, *Chem. Eng. Sci.,* **61**(18), 6035 (2006).
61. P. Sivakumar, R. P. Bharti and R. P. Chhabra, *Chem. Eng. Sci.*, **62**(6), 1682 (2007).
62. R. P. Bharti, R. P. Chhabra and V. Eswaran, *Ind. Eng. Chem. Res.*, **46**(11), 3820 (2007).
63. R. C. Patil, R. P. Bharti and R. P. Chhabra, *Ind. Eng. Chem. Res.*, **47**(5), 1660 (2008).
64. R. C. Patil, R. P. Bharti and R. P. Chhabra, *Ind. Eng. Chem. Res.*, **47**(23), 9141 (2008).
65. F. B. Tian, R. P. Bharti and Y. Q. Xu, *Comput. Mech.*, **53**(2), 257 (2014).
66. K. M. Gangawane, R. P. Bharti and S. Kumar, *J. Taiwan Inst. Chem. Eng.* (2015), DOI:10.1016/j.jtice.2014.11.020.
67. K. Stephan and M. Abdelsalam, *Int. J. Heat Mass Transfer*, **23**, 73 (1980).